remote sensing

MDPI

Article

Urban Tree Classification Based on Object-Oriented Approach and Random Forest Algorithm Using Unmanned Aerial Vehicle (UAV) Multispectral Imagery

Qian Guo [1], Jian Zhang [1], Shijie Guo [1], Zhangxi Ye [1], Hui Deng [2], Xiaolong Hou [1,3,4] and Houxi Zhang [1,3,4,*]

[1] Forestry College, Fujian Agriculture and Forestry University, Fuzhou 350028, China
[2] College of Earth Sciences, Chengdu University of Technology, Chengdu 610059, China
[3] Key Laboratory of State Forestry and Grassland Administration for Soil and Water Conservation in Red Soil Region of South China, Fuzhou 350002, China
[4] Cross-Strait Collaborative Innovation Center of Soil and Water Conservation, Fuzhou 350002, China
* Correspondence: zhanghouxi@fafu.edu.cn

Abstract: Timely and accurate information on the spatial distribution of urban trees is critical for sustainable urban development, management and planning. Compared with satellite-based remote sensing, Unmanned Aerial Vehicle (UAV) remote sensing has a higher spatial and temporal resolution, which provides a new method for the accurate identification of urban trees. In this study, we aim to establish an efficient and practical method for urban tree identification by combining an object-oriented approach and a random forest algorithm using UAV multispectral images. Firstly, the image was segmented by a multi-scale segmentation algorithm based on the scale determined by the Estimation of Scale Parameter 2 (ESP2) tool and visual discrimination. Secondly, spectral features, index features, texture features and geometric features were combined to form schemes S1–S8, and S9, consisting of features selected by the recursive feature elimination (RFE) method. Finally, the classification of urban trees was performed based on the nine schemes using the random forest (RF), support vector machine (SVM) and k-nearest neighbor (KNN) classifiers, respectively. The results show that the RF classifier performs better than SVM and KNN, and the RF achieves the highest accuracy in S9, with an overall accuracy (OA) of 91.89% and a Kappa coefficient (Kappa) of 0.91. This study reveals that geometric features have a negative impact on classification, and the other three types have a positive impact. The feature importance ranking map shows that spectral features are the most important type of features, followed by index features, texture features and geometric features. Most tree species have a high classification accuracy, but the accuracy of *Camphor* and *Cinnamomum Japonicum* is much lower than that of other tree species, suggesting that the features selected in this study cannot accurately distinguish these two tree species, so it is necessary to add features such as height in the future to improve the accuracy. This study illustrates that the combination of an object-oriented approach and the RF classifier based on UAV multispectral images provides an efficient and powerful method for urban tree classification.

Keywords: multispectral image; Unmanned Aerial Vehicle (UAV); random forest; tree species classification; object-oriented

Citation: Guo, Q.; Zhang, J.; Guo, S.; Ye, Z.; Deng, H.; Hou, X.; Zhang, H. Urban Tree Classification Based on Object-Oriented Approach and Random Forest Algorithm Using Unmanned Aerial Vehicle (UAV) Multispectral Imagery. *Remote Sens.* **2022**, *14*, 3885. https://doi.org/10.3390/rs14163885

Academic Editors: Damir Klobučar, Mateo Gašparović and Ivan Pilaš

Received: 7 July 2022
Accepted: 9 August 2022
Published: 11 August 2022

1. Introduction

As an essential part of the city, urban trees provide many ecological, economic, and social benefits to the people living and working in the cities [1–3]. With the deepening of urbanization, the ecological benefits of urban trees have become prominent. However, the ecological benefits of urban trees may vary significantly with different tree species, planting structures and location environments [4]. Therefore, to optimize the management of urban trees to maximize their ecological value, it is necessary to acquire accurate and timely information about their species and distribution. Moreover, the information about their

species and location also plays a vital role in running the ecological models and achieving an accurate assessment of their ecological value [5]. Therefore, it is vital to explore the means to accurately and timely identify the species and map the distribution of urban trees.

Traditionally, the collection of tree information has primarily relied on labor-intensive field surveys, which are inefficient and costly. With the development of remote sensing technology, satellite-based remote sensing has become a critical alternative for tree identification, for it can attain images of a large area once [6]. However, it has the disadvantages of an extended return period, low resolution, high price, and fixed orbit, which cannot meet the requirements of tree monitoring [7]. The standard remote sensing platform has gradually transformed into a small and lightweight Unmanned Aerial Vehicle (UAV) platform. Since the flight height of the UAV, generally dozens to hundreds of meters above the ground, is much lower than that of other aerial platforms, it can provide a higher spatial resolution and effectively reduce the impact of clouds on the image quality [8]. Recently, UAV technology has been used for various remote sensing applications such as agriculture, hydrology, and ground deformation monitoring [9–11]. Moreover, the UAV is more flexible and has a shorter return cycle, as it can fly according to the route set by the user. The UAV can be equipped with sensors of different kinds, such as RGB, multispectral, hyperspectral and LiDAR [8]. Although UAVs equipped with hyperspectral and LiDAR sensors can provide more spectrum features or structural information, they also cost more, restricting their promotion and application in various fields [12]. Similarly, UAVs equipped with RGB sensors possess the characteristics of high temporal and spatial resolution and low cost [13]. Still, they are able to provide far less spectrum information than a hyperspectral sensor, thus limiting their application in recognition of various targets, especially in vegetation discrimination [14]. Otherwise, UAVs equipped with multispectral sensors can attain an image with more spectrum features than possible with RGB, while also having a much lower cost than that of hyperspectral sensors and LiDAR, thus representing a good balance between price and image quality, which shows irreplaceable advantages in identification of complex tree species and promising potential with respect to their promotion.

Traditional classification methods are mainly based on the pixel, utilizing only the spectral features of various pixels [15]. Therefore, pixel-based classification methods are prone to the salt-and-pepper phenomenon, that is, the same category will be classified into different categories due to the considerable spectral variation. In contrast, object-oriented methods, which use homogenous objects obtained through segmentation instead of pixels as a classification unit, can make full use of other features [16], such as geometric features, texture features, etc. However, this may lead to a high degree of data redundancy, as the dimensions of the features used in object-oriented classification methods increase significantly. The capacity of traditional algorithms is limited when dealing with high-dimensional data, and therefore it is necessary to develop new algorithms. Random forest (RF) is a new algorithm that integrates multiple trees based on the idea of ensemble learning, and it can handle thousands of input variables without reduction and evaluate the importance of input variables [6]. It is good at processing non-parametric and high-dimensional data, and has a solid anti-overfitting ability and a high computational efficiency. It has been widely used in biology, medicine, remote sensing, and other fields [17–19].

Because object-oriented methods and the RF algorithm have their own advantages in data processing, many scholars have recently tried to combine them to perform image classification in remote sensing. Jean et al. [20] developed a wetland inventory of the Conne River watershed using an object-oriented method and RF with an overall accuracy (OA) of 92% and a Kappa coefficient (Kappa) of 0.916. Comparing multiple classifiers, Wang et al. [21] found that the method based on an object-oriented approach and the random forest classifier attained a higher accuracy of 91.3% at the single tree scale. Although some achievements have been made in studies based on object-oriented and random forest methods, the current studies are primarily in wild regions where trees occur in large patches and are generally spread over a large expanse to form a huge forest. However, the urban environment is much more complex than wild regions, as trees are usually scattered around

buildings and roads. The enormous environmental differences that make the methods of tree classification suitable for wild areas not applicable to urban tree identification. Moreover, most of the current research presenting satisfactory results is based on expensive hyperspectral data, and fewer studies are based on UAV multispectral data.

In this study, we performed urban tree classification based on a method combining an object-oriented approach and a random forest algorithm using UAV multi-spectral imagery. The main objectives of this study were: (1) to compare the performance of RF and the other two algorithms support vector machine (SVM) and k-nearest neighbor (KNN) under various schemes; (2) to determine the importance of different features in the classification of urban trees; and (3) to map the distribution of urban trees based on the optimal scheme for every algorithm. It is expected that through the verification and analysis of the classification method, a practical and efficient identification method of urban tree species can be obtained, providing a reference for the monitoring, management, and protection of urban trees.

2. Materials and Methods

2.1. Study Area

The study area (119°51′E, 26°07′N) is located in the Mawei District, Fuzhou City, Fujian Province, China (Figure 1). This area is characterized by a semi-tropical monsoon climate with an annual sunshine duration of 1700~1980 h, an average annual temperature of 18~26 °C and an annual rainfall of 900~2100 mm. The study area is very flat, with an altitude of 9 m (ASL). The main tree species in the study area are *Banyan*, *Eucalyptus*, *Willow*, *Alstonia scholoris*, *Camphor*, *Cinnamomum Japonicum*, and *Palmae plants*, which are typically representative of urban trees in Fuzhou city.

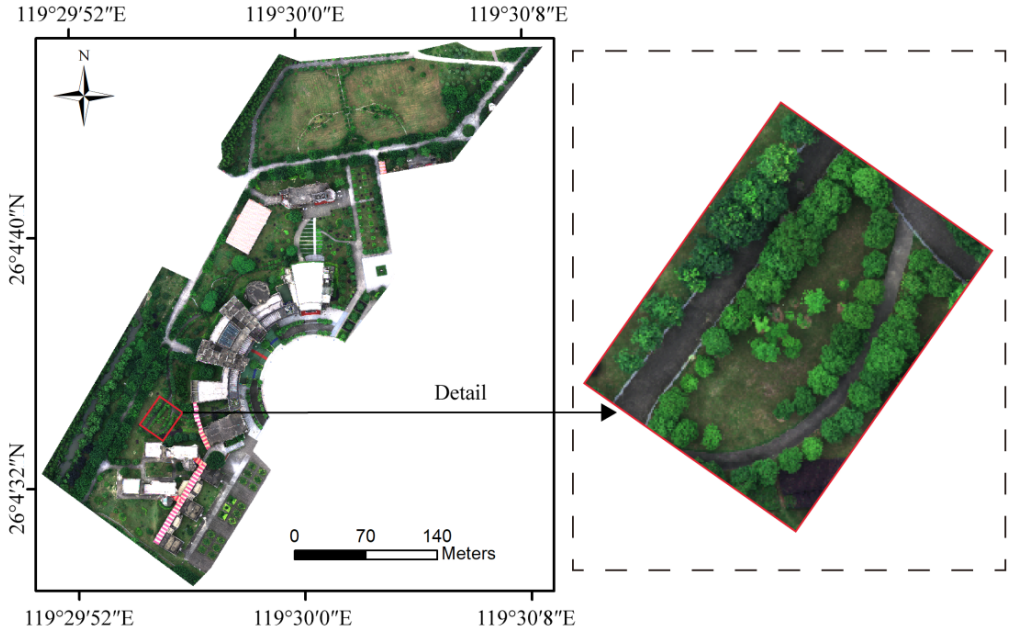

Figure 1. The RGB image of the study area.

2.2. UAV Image Acquisition and Preprocessing

The aerial photography was performed using a DJI UAV (DJI Technology Co., Ltd., Shenzhen, China) on 11 June 2021. To avoid the influence of shadows, we chose a period with sufficient light and cloud for aerial photography, and the data were acquired during the time from 10:00 am to 15:30 pm. The UAV was equipped with five multispectral camera lenses (blue: 450 ± 16 nm, green: 560 ± 16 nm, red: 650 ± 16 nm, red edge: 730 ± 16 nm, near-infrared: 840 ± 26 nm), each of which had a resolution of 2 million (1600 × 1300) pixels. The route planning was completed using DJI Pro (DJI Technology Co., Ltd., Shenzhen, China) with a flight altitude of 60 m, a heading overlap of 70%, and a side overlap of 65%.

A total of 6846 images were acquired, of which each position contained 1 RGB image and 5 single-band images, and the spatial resolution of each image was about 0.01 m. The software DJI Terra 2.3.3 (DJI Technology Co., Ltd., Shenzhen, China) was used to construct an image mosaic, the ENVI5.3 was used for stacking of single-band images and image cropping, and an orthophoto image with a spatial resolution of about 0.01 m was produced. The true color image of the study area is shown in Figure 1.

2.3. Research Methods

In this study, a method for urban tree classification using an object-based approach and machine learning algorithms based on UAV multispectral images is proposed. The classification process mainly consists of the following four steps (Figure 2): (1) segmentation, which includes segmentation scale selection and image segmentation; (2) feature combination, in which 9 schemes have been designed, where S1–S8 were designed based on feature combination, and S9 contains all the preferred features; (3) classification implementation, in which the RF, KNN and SVM classifier are used to classify the tree species; (4) accuracy evaluation, in which the OA, Kappa and F1-Score are selected to evaluate the classification accuracy; and (5) random forest classification result analysis.

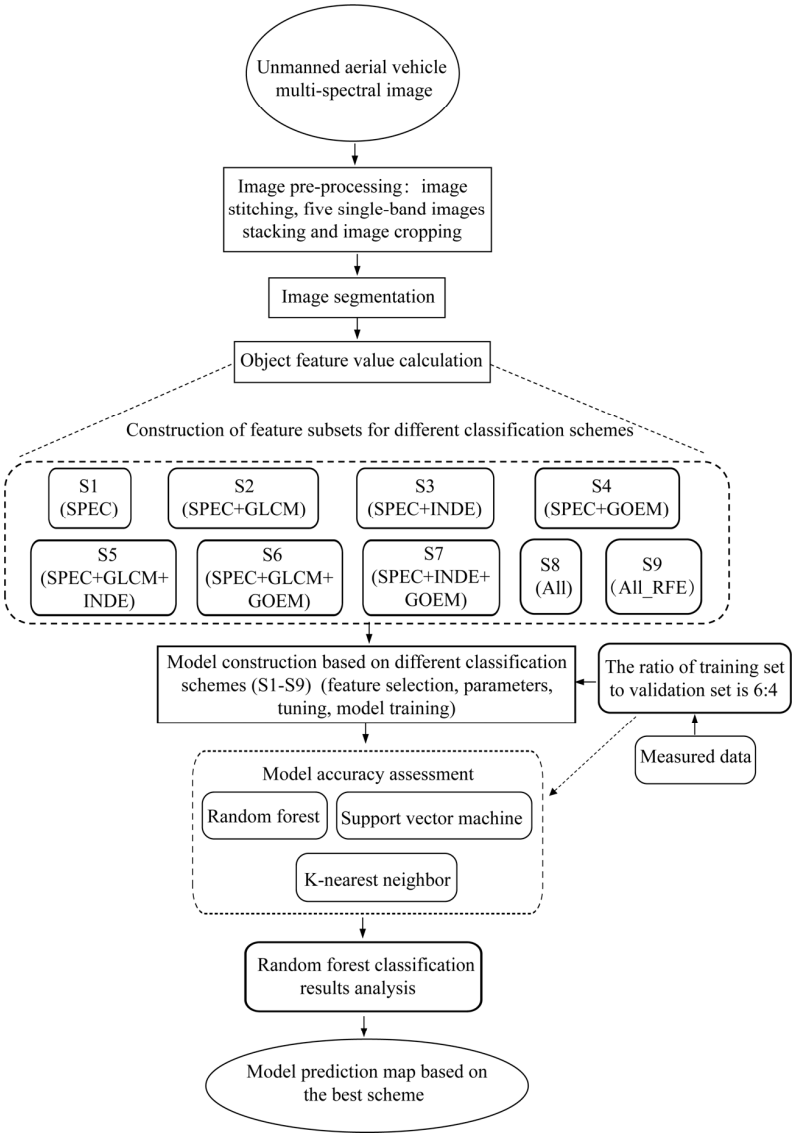

Figure 2. Technical flow chart.

2.3.1. Image Segmentation

Recently, the object-oriented approach has been increasingly applied to remote sensing image classification. Segmentation is the first step in object-oriented classification, and the results directly influence the classification accuracy. Three main parameters must be set: scale, shape, and compactness. If the scale is too large, it will lead to incomplete image segmentation, resulting in multiple categories within one object. If the scale parameter is too small, the image segmentation will over-segment and increase classification difficulty. In this study, the ESP2 tool combined with visual identification was used to confirm the optimal scale and all image segmentation processes were done in eCognition Developer 9.0 software (Trimble Germany GmbH, Munich, Germany). The quantitative evaluation indicators of the ESP2 is local variance (LV) and rates of change of LV. When the value of the change rate of LV reaches its maximum, the segmentation scale corresponding to this point is a relatively optimal segmentation scale. Images were segmented on eCognition using alternate scales obtained by the ESP2 tool, and the final scale was determined by visually comparing the segmentation effects.

2.3.2. Object Features

a. Spectrum features (SPEC) include the average or standard deviation of the five bands (blue, green, red, red edge and near-infrared), the maximum difference, and overall brightness value, amounting to 12 in total.
b. Index features (INDE) include RGR, VARI, SIPI, SR, TVI, NDGI, NDVI, NDWI, CIWI, MSWI, DVI, RVI, amounting to 12 in total (Table 1).

Table 1. The formula of index features.

Index Features	Formula	Reference
CIWI	NDVI + RE	[22]
DVI	NIR − RE	[23]
NDVI	(NIR − R)/(NIR + R)	[24]
NDGI	(NIR − G)/(NIR + G)	[25]
NDWI	(G − NIR)/(G + NIR)	[26]
RGR	R/G	[27]
SR	NIR/RE	[28]
SIPI	(NIR − B)/(NIR + B)	[29]
VI_{opt}	1.45 × (NIR × NIR + 1)/(RE + 0.45)	[30]
TVI	60 × (NIR − G)/100 × (NIR + G)	[31]
VARI	(G − R)/(G + R)	[32]
GOSAVI	(1 + 0.16) × (NIR − G)/(NIR + G + 0.16)	[33]

c. Texture features (GLCM) include mean (GLCM_Mean_All), standard deviation (GLCM_SD_All), entropy GLCM_Ent_All), homogeneity (GLCM_Homo_All), contrast (GLCM_Con_All), dissimilarity (GLCM_Diss_All), angular second moment (GLCM_Ang_All) and correlation of Gray-level co-occurrence matrix (GLCM_Corre_All), amounting to 8 in total (Table 2).

Table 2. Formula and description of GLCM features.

Feature Type	Formula	Parametric Descriptions
Mean	$\sum_{i=0}^{quant_k} \sum_{j=0}^{quant_k} p(i, j) \times i$	Degree of texture regularity
Standard deviation	$\sqrt{\sum_{i=0}^{quant_k} \sum_{j=0}^{quant_k} p(i, j) \times (i - Mean)}$	Deviation between pixel gray value and mean

Table 2. *Cont.*

Feature Type	Formula	Parametric Descriptions
Entropy	$\sum_{i=0}^{quant_k}\sum_{j=0}^{quant_k} p(i, j) \times \ln p(i, j)$	Measures the degree of the disorder among pixels in the image
Homogeneity	$\sum_{i=0}^{quant_k}\sum_{j=0}^{quant_k} p(i, j) \times \frac{1}{1+(i+j)^2}$	Texture uniformity
Contrast	$\sum_{i=0}^{quant_k}\sum_{j=0}^{quant_k} p(i, j) \times (i-j)^2$	Measures the contrast based on the local gray level variation
Dissimilarity	$\sum_{i=0}^{quant_k}\sum_{j=0}^{quant_k} p(i, j) \times \lvert i-j \rvert$	Texture contrast
Angular second moment	$\sum_{i=0}^{quant_k}\sum_{j=0}^{quant_k} p(i, j)^2$	Measures the uniformity or energy of the gray level distribution of the image
Correlation	$\sum_{i=0}^{quant_k}\sum_{j=0}^{quant_k} \frac{(i-Mean)\times(j-Mean)\times p(i, j)^2}{Variance}$	Measures the linear dependency of gray levels of neighboring pixels

Note: here, i, j are the rank coordinates of the element in the image, $p(i, j)$ is the gray joint probability matrix, and $quant_k$ is the order of gray-level co-occurrence matrix.

d. Geometric features (GEOM) include area, length/width, length, width, border length (Border_length), shape index (Shape_index), density, main direction (Main_direction), asymmetry, roundness, boundary index (Border_index), number of pixels (No_pix), compactness, volume, ellipse fitting, rectangle fitting (Rect_Fit), maximum ellipse radius (Rad_largest_ellipse), minimum ellipse radius (Rad_smallest_ellipse), amounting to 18 in total.

2.3.3. Sub-Feature Sets Construction for Different Schemes

To understand the effects of different features on the classification result, nine kinds of feature subsets were built to form nine different classification schemes in this study (Table 3). S1 contains only spectral features, while S2 (SPEC + GLCM) and S3 (SPEC + INDE) add texture features and index features based on spectral features, respectively. S4 (SPEC + GEOM) contains spectral features and geometric features, while S5 (SPEC + GLCM + INDE) and S6 (SPEC + GLCM + GEOM) add index features and geometric features based on S2, respectively. S7 (SPEC + INDE + GEOM) adds geometric features based on S3, S8 (All) includes all feature types and S9 (All_RFE) includes features selected by the recursive feature elimination (RFE) method [34].

Table 3. The feature subsets of various schemes.

ID of Schemes	Feature Subsets	SPEC	GLCM	INDE	GEOM	Total Features
S1	SPEC	12				12
S2	SPEC + GLCM	12	8			20
S3	SPEC + INDE	12		12		24
S4	SPEC + GEOM	12			18	30
S5	SPEC + GLCM + INDE	12	8	12		32
S6	SPEC + GLCM + GEOM	12	8		18	38
S7	SPEC + INDE + GEOM	12		12	18	42
S8	All	12	8	12	18	50
S9	All_RFE	12	6	12		30

Note: All_RFE consists of features optimized by the RFE method, including GLCM_SD_All, GLCM_Corre_All, GLCM_Con_All, GLCM_Homo_All, GLCM_Diss_All, GLCM_Mean_All, all spectral features, and index features.

2.3.4. Training and Verification Samples

According to the approximate area of different categories in the image, the sampling number of twelve categories was determined (Table 4). The total number for different categories ranged from 60 to 150. To ensure that the proportion of each category in the training dataset is consistent with that in the verification dataset, the stratified sampling method was used to construct the training and the verification dataset. Random sampling was adopted for each category at a ratio of 6:4 (Table 4), among which the training sample (60%) was used to build the classification model, and the verification sample (40%) was used to verify the classification accuracy.

Table 4. Training and validation samples.

Category	Total Samples	Training Samples	Validation Samples
Alstonia scholaris	90	54	36
Banyan	150	90	60
Camphor	80	48	32
Eucalyptus	110	60	40
Willow	90	54	36
Cinnamomum japonicum	90	54	36
Palmae plants	80	48	32
Shrub	140	84	56
Lawn	160	96	64
Building	150	90	60
Road	150	90	50
Water	60	36	24

2.3.5. Classifier

RF is a non-parametric learning method whose classification results are determined by multiple decision trees. Compared with other classifiers, RF has the advantages of being less prone to overfitting and reducing the impact of outliers, leading to higher accuracy of the classification in many studies. There are two important parameters for the RF classifier: the number of decision trees (ntree) and the number of features contained in each decision tree (mtry). Firstly, the number of decision trees was set as 1000, and the mtry was traversed from 0 to 50 with an interval of 1 to determine the optimal mtry based on the out-of-bag (OOB) error rate. Then, the number of features was set to the optimal value, and the ntree was traversed from 0 to 1000 with an interval of 1, and the number of decision trees with the smallest out-of-bag error was the optimal value. The importance of the features in each classification scheme was determined based on the mean decrease in accuracy.

SVM is a generalized linear classifier that performs binary classification on data according to the supervised learning method, and its decision boundary is the maximum margin hyperplane that solves the learning sample [34]. KNN is a non-parametric method that assumes that elements of similar classes are close to each other. The distance of the unknown object from the k nearest neighbors can be measured. If most of the k nearest samples near the unknown sample belong to a certain category, the unknown sample would also be classified as the category [35].

The RF, SVM and KNN algorithms were performed by the randomForest, e1071 and kknn packages of R programming language, respectively.

2.3.6. Accuracy Evaluation

To evaluate the classification accuracy of the model, the OA [36], Kappa [36] and F1-Score [37] are chosen which could be calculated based on the confusion matrix. The OA is a ratio representing the number of correctly classified samples to the total number, which is between 0 and 1. The closer the ratio is to 1, the higher the classification accuracy. The Kappa measures the consistency between the true category and the predicted one by the model. The higher the Kappa, the higher the classification accuracy. The F1-Score

comprehensively considers the recall rate and the precision rate, and the recall rate is high, indicating that the model is more inclined to regard a sample as a positive sample. A high precision rate means that the model is more cautious in predicting. F1-Score is a weighted average evaluation index, with a value range of [0, 1]. The closer the value is to 1, the higher the accuracy. The calculation formula is as follows, respectively.

$$\mathrm{OA}(\%) = \frac{\sum_{i=1}^{n} P_{ii}}{N} \times 100 \quad (1)$$

$$\mathrm{Kappa} = \frac{N\sum_{i=1}^{n} P_{ii} - \sum_{i=1}^{n}(P_{i+} \times P_{+i})}{N^2 - \sum_{i=1}^{n}(P_{i+} \times P_{+i})} \quad (2)$$

$$\mathrm{UA}(\%) = \frac{P_{ii}}{P_{i+}} \times 100 \quad (3)$$

$$\mathrm{PA}(\%) = \frac{P_{ii}}{P_{+i}} \times 100 \quad (4)$$

$$\mathrm{F1} = \frac{2 \cdot UA \cdot PA}{UA + PA} \quad (5)$$

In the formula, n is the total number of classes, N is the total number of validation samples, P_{ii} is the number of correctly classified samples in the i-th row and i-th column of the confusion matrix, P_{i+} and P_{+i} are the total number of samples in the i-th row and i-th column.

Since the result of each run of the RF would have a slight difference, after determining the optimal values of the number of features and the number of decision trees, each model was run 2000 times before its accuracy is evaluated.

3. Results

3.1. Image Segmentation in eCognition

The estimation results of the scales using the ESP2 tool are shown in Figure 3. Six peak values, including 115, 125, 142, 188, 275 and 285, were selected as alternatives to the optimal scales. By examining the segmentation results based on those scales (Figure 4), it can be seen that the urban trees were over-segmented at scales from 115 to 188, while they were segmented well at scales of 275 and 285. Carefully comparing the segmentation effects based on the two scales (275 and 285), we finally chose 275 as the optimal segmentation scale. The shape index and compactness were set to 0.1 and 0.5 after comprehensively considering the topography of the study area and the distribution of the objects to be classified.

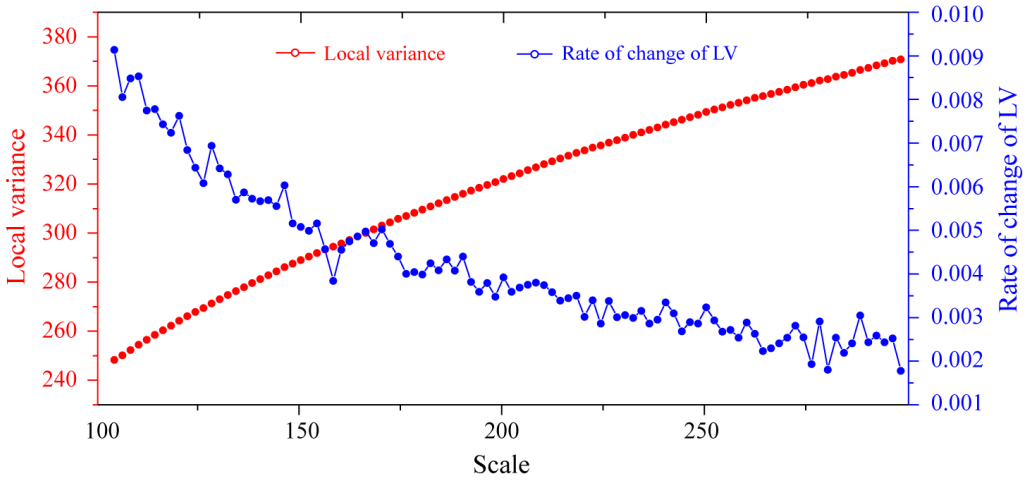

Figure 3. The estimation of the scales using the ESP2 tool.

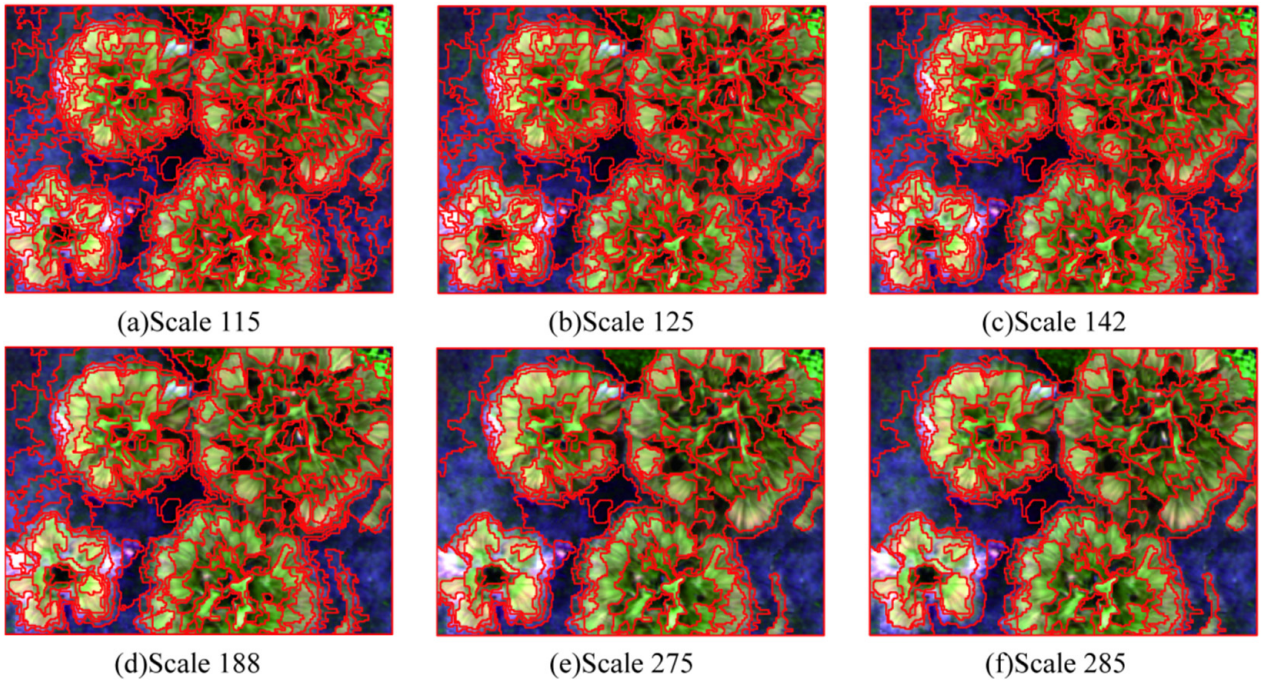

Figure 4. Segmentation results based on different scales.

3.2. RF Parameter Tuning

The results of RF parameter tuning showed that, when the decision tree was set to 1000, the OOB error rates of different schemes showed a similar trend of first decreasing and then fluctuating as the number of features increased (Figure 5). When the OOB error rate of each scheme reached the lowest value, its corresponding number of selected features was the optimal value. Based on the optimal number of features, the OOB error rates of all schemes showed a similar trend, decreasing first and then fluctuating within a small range, as the number of decision trees increased. The best combination of the number of features and decision trees for S1, S2, S3, S4, S5, S6, S7, S8 and S9 were (2, 747), (7, 154), (6, 985), (9, 612), (14, 546), (12, 885), (15, 294), (30, 176), and (16, 770), respectively.

3.3. Accuracy Assessment

The classification results indicate that RF has a higher OA and Kappa than SVM and KNN in every scheme (Figure 6). In S9, with the highest accuracy among all schemes, the OA of RF is 4.67 and 4.49 percentage points higher than that of SVM and KNN, respectively. Therefore, it can be seen that the RF algorithm performs better at urban tree identification than the other two.

The best result for the RF was achieved in S9, with an OA of 91.89% and a Kappa of 0.91, and S8 also achieved high accuracy, with an OA of 91.15% and a Kappa of 0.90. However, the accuracy of S8 using all features was lower than that of S9 using only the preferred feature set. It can be seen that feature optimization using the RFE method is conducive to improving accuracy. Analyzing the changes in accuracy, it can be found that different feature sets have different effects on accuracy. Adding index features and texture features based on S2 and S3, the OA increased by 5.4% and 2.5%, respectively. However, by introducing geometric features based on S2 and S3, the OA was decreased by 0.6% and 0.1%, respectively, which shows that index and texture features have a positive impact on OA, while geometric features have a negative impact on OA.

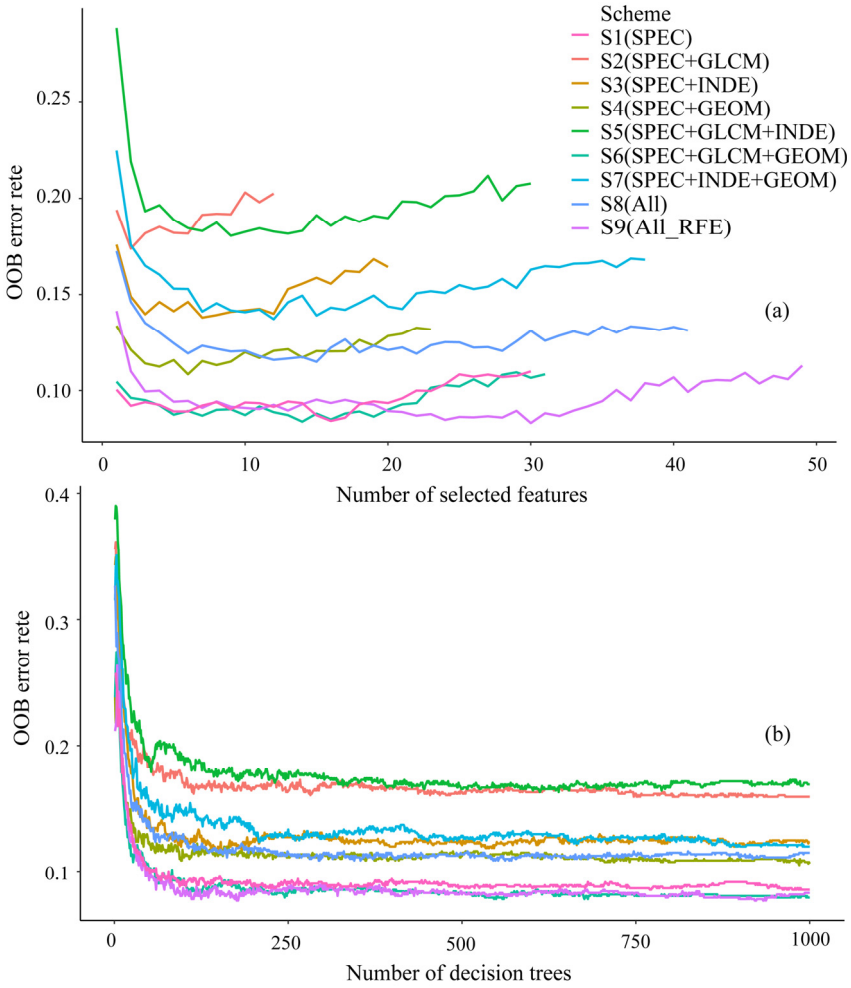

Figure 5. Out-of-bag (OOB) error rate of different numbers of features (**a**) and different numbers of decision trees (**b**) for various schemes.

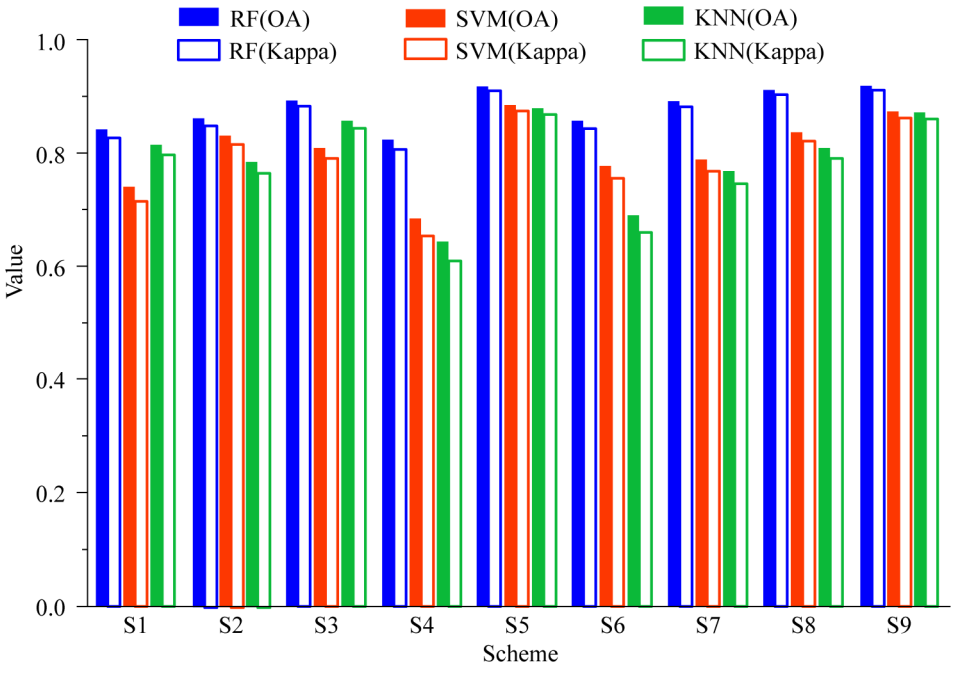

Figure 6. The overall classification accuracy and Kappa of different classifiers and different schemes.

As shown in Figure 7, the classification accuracy of each category varies significantly. It can be seen that the accuracy for tree species is slightly lower than that for non-tree species. The accuracy for most tree species is larger than 90%, while the accuracy for *Cinnamomum japonicum* and *Camphor* is lower than other tree species. The accuracy for *Camphor* is mostly less than 80%, which is far lower than that for other tree species, and the accuracy for *Cinnamomum japonicum* is even lower than 70% in S1 and S4. It is worth noting that the addition of geometric features leads to a significant decrease in the accuracy of almost all categories, which shows that geometric features play a negative role in urban tree classification.

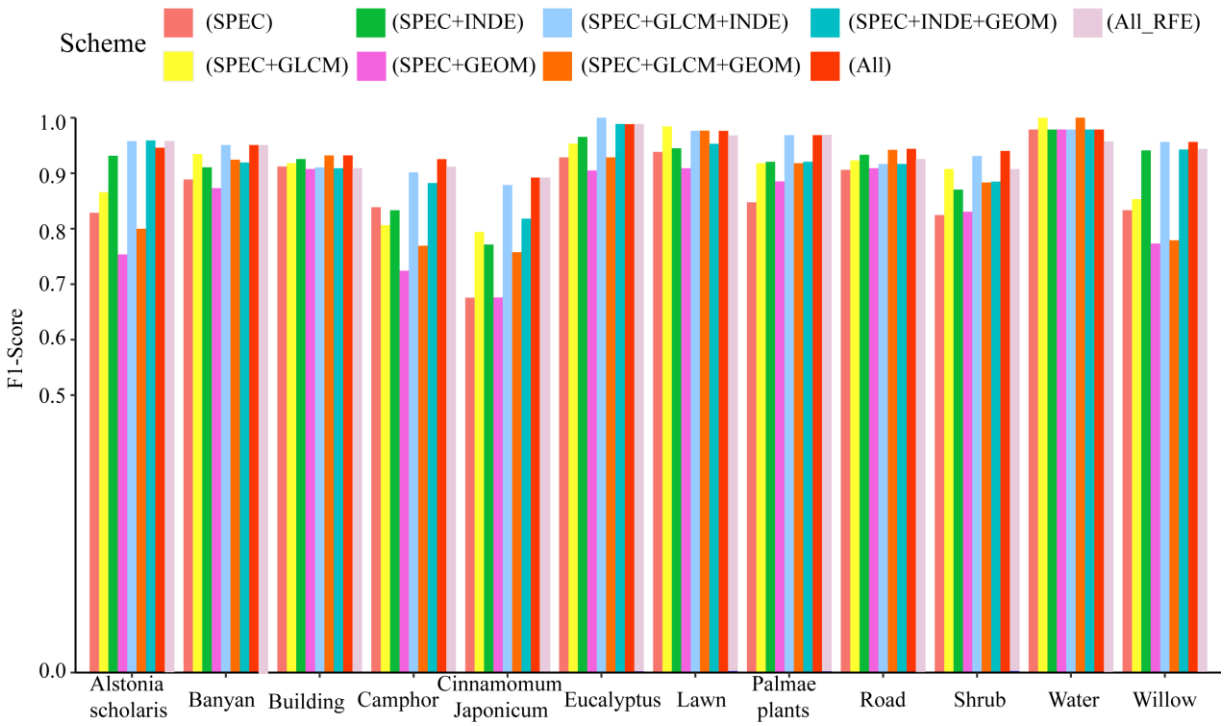

Figure 7. F1-Score of different schemes for different vegetable categories.

3.4. Feature Importance

The feature importance results show that different feature types play different roles in urban tree classification (Figure 8). The importance of spectral features and index features is more similar. Still, it can be observed that when the scheme has both spectral features and index features among the top 20 important features, the number of spectral features is always slightly greater than that of index features, which means that spectral features are relatively more important. Texture features are less important than spectral and index features, because there are no more than five texture features in the top 20 most important ones in S5, S6, S8 and S9, and the ranking of texture features is lower than spectral and index features, as well. The geometric features are the least important features among the four selected, for neither S8 nor S9 have geometric features in the top 20. Therefore, among the four types of feature, the spectral features are the most important ones, followed by the index features, texture features, and geometric features.

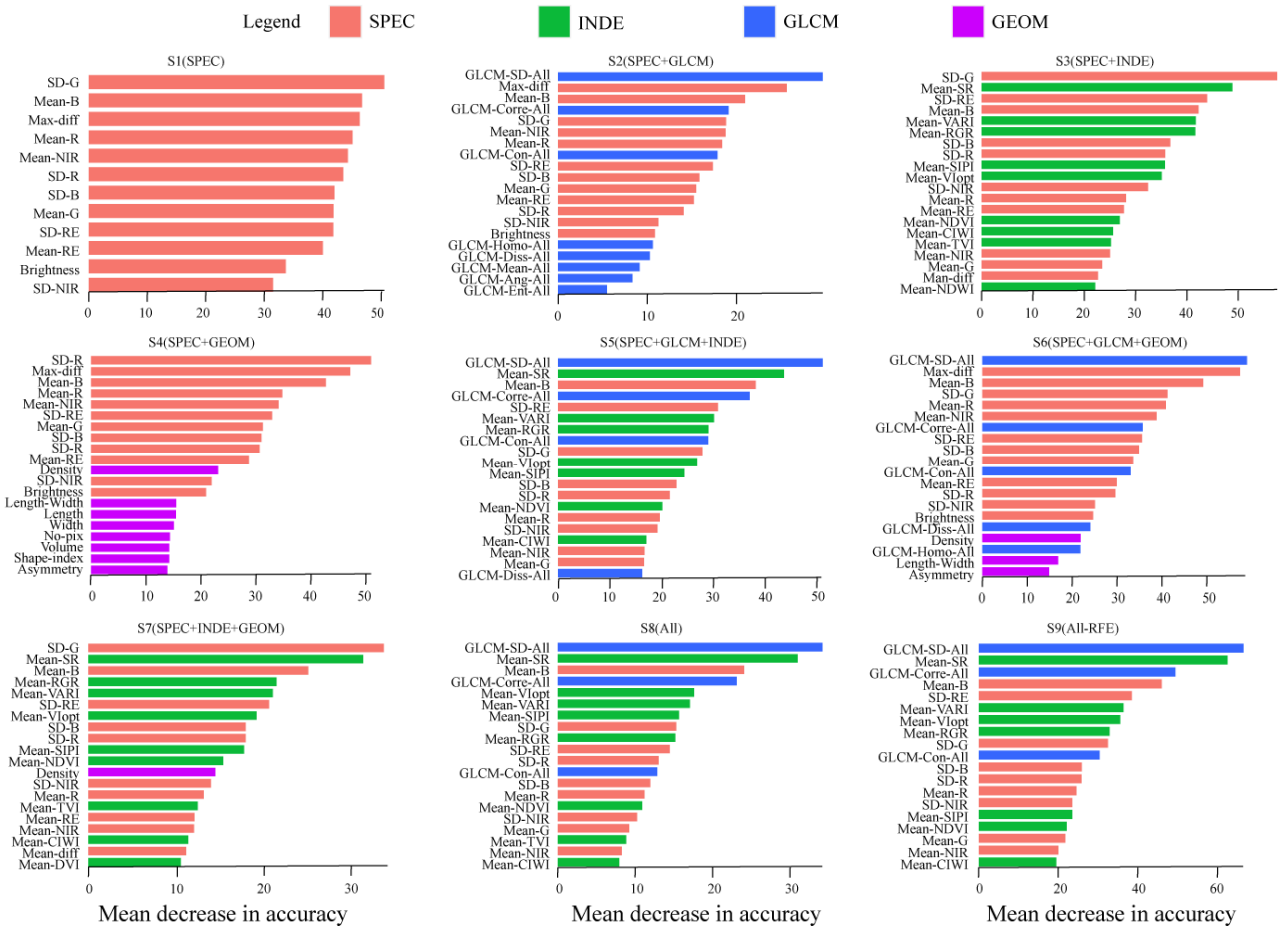

Figure 8. The twenty most important features for models S1–S9 (only 12 for S1).

Although SD_G (SPEC) ranked first in some schemes (S1, S3, S4 and S5), it is evident that the GLCM_SD_All (GLCM) is the most important feature for discriminating tree species, for GLCM_SD_All has a higher ranking when there are both spectral features and texture features in the scheme. Mean_SR (INDE), Mean_B (SPEC), GLCM_Corre_All (GLCM), SD_RE (SPEC) and Max_diff (SPEC) also rank higher in the top 20 important features. Generally, each feature in the spectral feature set shows a similar ranking in different schemes. Mean_SR, an index feature combined with the near-infrared band and the red-edge band, ranks first among all the index features, which means that both the near-infrared band and the red-edge band play a significant role in tree species identification.

3.5. Classification Map of the Study Area

The classification map of the study area of each classifier (RF, SVM and KNN) based on the best scheme shows that the RF classifier performs better than the other two (Figure 9). Generally, the RF could accurately identify most of the tree species. It can be seen from the enlarged image that the RF algorithm was able to accurately recognize *Willow*, while there was a higher rate of misclassification for the other two classifiers, especially for SVM. In terms of non-tree species recognition, RF also had the highest accuracy. RF was able to identify most buildings and roads, while SVM and KNN failed to make a complete identification for the building and also misclassified many roads as belonging to the grass category. From the classification prediction map, it can be seen that RF was able to identify both tree species and non-tree species with higher accuracy than the SVM and KNN algorithms.

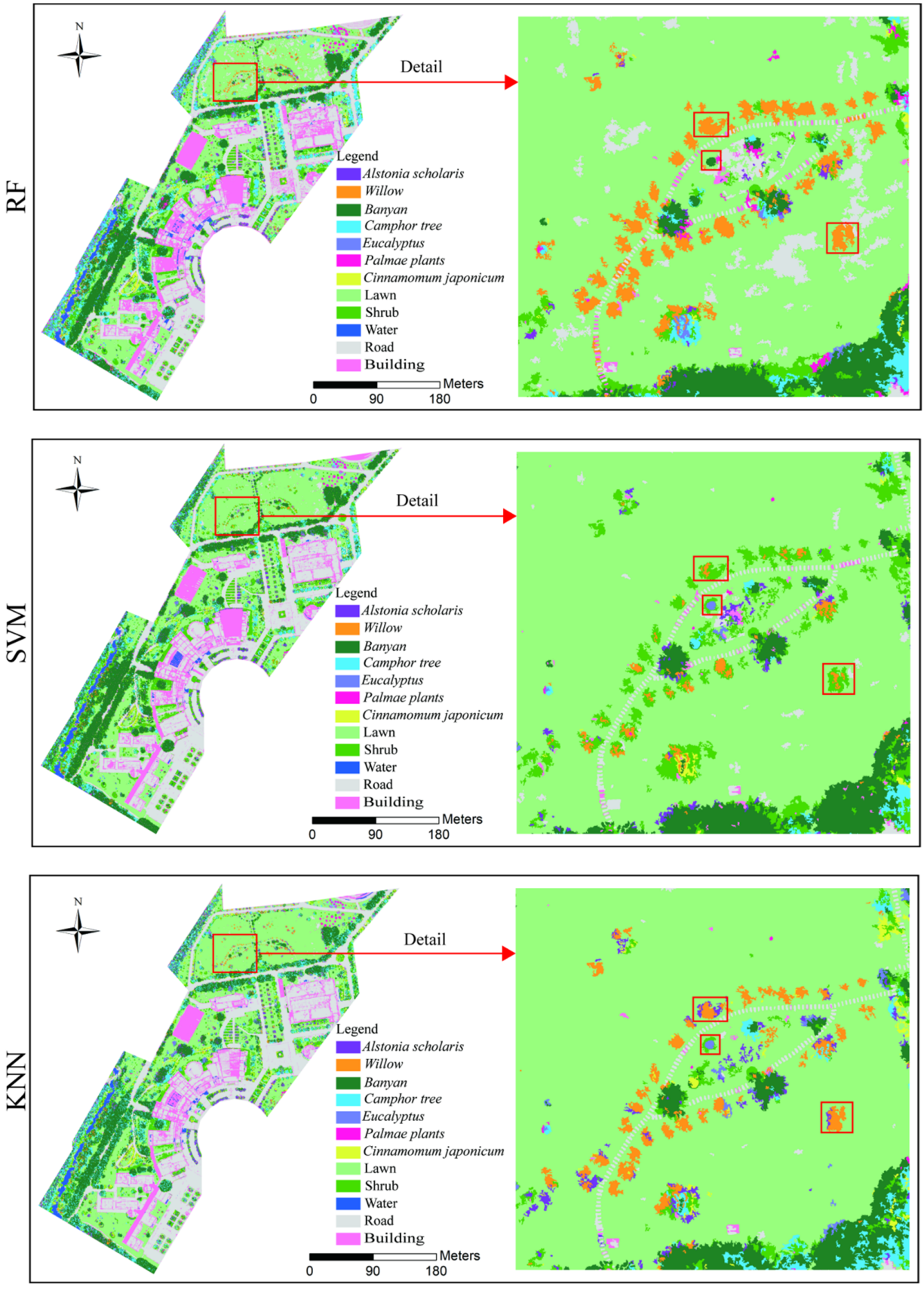

Figure 9. Classification results of each classifier (RF, SVM and KNN) based on the best scheme.

4. Discussion

Our study indicated that the RF classifier performed better than SVM and KNN in the tree classification. This is consistent with many research results indicating that RF has higher accuracy than SVM and KNN [34,35]. The RF classifier provides its final classification result by means of a vote from its multiple decision trees. Therefore, it can process high-dimensional data directly and could be less affected by noise [36]. The SVM seeks the optimal classification surface in the case of linear separability. It was initially proposed to solve the binary classification problem, but there are some limitations when applied to multi-category classification [38]. The KNN is a simple and easy-to-implement classification algorithm that mainly performs classification on the basis of the similarity between training samples and test samples [39]. However, if the objects to be classified in the study area are complex, it is prone to misclassification and omission. Therefore, the RF classifier, with a strong anti-overfitting and strong generation ability, is a suitable option for tree species identification, and it can still give stable results even with more complex datasets. In addition to SVM and KNN, artificial neural network (ANN) is also a hotspot algorithm for land-use/land-cover mapping, yet many studies indicate that RF has a higher accuracy than ANN [40].

The accuracy of each scheme for the RF classifier varies greatly, and S9 achieved the best classification results among all nine schemes. A possible reason for this is that S9 has the preferred feature set through the recursive feature elimination method, which not only retains the important features for classification, but also eliminates feature redundancy, improving model performance. It can be found that the introduction of geometric features leads to a decrease in accuracy in the various schemes, which means that the geometric features have a negative effect on classification accuracy. Geometric features, including width, area, length, and other information, not only provide useful information for tree species identification, but also lead to feature redundancy due to the increase in the number of features, resulting in reduced accuracy [39,41]. The segmentation scale is an important factor affecting accuracy for object-oriented classification [42]. Although ESP2 was selected to assist in determining the optimal segmentation scale in this study, the ESP2 could only provide several alternatives for optimal scales, and the final optimal scale still needs to be determined through visual discrimination, which cannot be completely objective or automated. In the follow-up research, it is necessary to explore the method of automatic determination of segmentation parameters to further increase accuracy and the level of automation.

The F1-Score was calculated to evaluate the ability of the RF classifier to identify every tree species. The results indicated that the *Camphor* and *Cinnamomum japonicum* had a lower F1-Score than other tree species, and the latter even had an F1-Score lower than 70% in S1 and S4. This may have occurred because *Camphor* and *Cinnamomum japonicum* both belong to the same family (Lauraceae), and possess similar leaf shape, tree-crown shape, and spectral characteristics. Therefore, the use of the spectral, index, texture and geometric features in the current study had little effect on distinguishing them accurately. However, the tree species have different heights, with the first one ranging from 12 to 17 m and the second one reaching 30 m, so the separability between them may be significantly increased with the inclusion of height features. Conversely, *Alstonia scholaris*, *Banyan*, *Eucalyptus* and *Palmae plants* have high F1-Score values. This may be because these four types of tree species have more obvious characteristics with respect to leaf shape and crown shape, and can be easily visually recognized and are difficult to mistakenly classify as other tree species. The non-tree categories all have higher F1-Scores, especially the water and lawn, with an F1-Score of close to 1.0 in every scheme. The F1-Score of roads and buildings are relatively lower, which may be accounted for by the fact that their shapes are rather similar and prone to causing misclassification.

This study shows that the most important features are spectral features, followed by index features, while texture features and geometric features play a relatively minor role, especially geometric features. In this study, texture and geometric features are added based

on spectral and index features to increase the amount of object information and obtain higher classification accuracy. However, the results show that the S8 based on all features has a lower accuracy than the preferred S9 based on partial features. Sothe et al. [43] also found a similar phenomenon whereby they attained the highest classification accuracy when using only a portion of the features (only 36), with an accuracy that was 1.7% higher than when using all features, indicating that more features does not always lead to higher accuracy. Other studies have shown that when a small number of features are used, the introduction of new features significantly increases the separability of categories, and when the number of features reaches a certain number, adding features will not lead to substantial improvement in the separability of categories [41]. After reaching the saturation point, adding features will usually lead to data redundancy, thus reducing model efficiency and affecting its performance. The RF classifier can build a preferred feature set through the feature importance to reduce computational cost and improve computational efficiency [44]. By analyzing the feature importance ranking map, it can be found that the NIR band and RE band play an important role in classifying urban trees, Abdollahnejad et al. [45] also found that the red-edge band is very important for tree species identification. This is because the reflectivity of plants increases sharply in the near-infrared band, and a reflection peak is formed at the red edge. Therefore, plants are sensitive to the NIR and RE bands, so the addition of these two bands is of great help to the identification of tree species.

5. Conclusions

In this study, we proposed a method for urban tree classification combining an object-oriented approach and a random forest algorithm based on UAV multi-spectral imagery. The results showed that the RF classifier performed better than the other two machine learning algorithms (SVM and KNN) in every scheme. The RF classifier achieved the highest accuracy when using the preferred feature set (S9), with an OA of 91.89% and a Kappa of 0.91. Different features have different effects on the classification results. Geometric features have a negative impact on the classification accuracy, while the other three types of features have a positive impact. Among these three types of features, spectral features have the greatest impact on classification accuracy, followed by index features and texture features. As for the specific features, GLCM_SD_All (GLCM), Mean_SR (INDE), Mean_B (SPEC), GLCM_Corre_All (GLCM), SD_RE (SPEC), and Max_diff (SPEC) rank higher in the top 20 most important features. Mean_SR is an index feature combined with the near-infrared band and the red-edge band, so both the near-infrared band and the red-edge band play a significant role in tree species identification. Most tree species achieved high accuracy, but *Camphor* and *Cinnamomum japonicum* are highly similar in appearance and spectral characteristics, and the selected features in this experiment were not able to accurately distinguish between them, resulting in a much lower accuracy than that obtained for other tree species. In future research, features such as height could be added to assist in identifying urban trees with similar appearances. The current study verified the effectiveness of the urban tree classification method based on UAV multispectral imagery and random forest classifier, providing a new technique for tree monitoring, management and protection in the city.

Author Contributions: Conceptualization, Q.G. and H.Z.; methodology, Q.G. and H.Z.; software, Q.G. and H.Z.; validation, Q.G., H.Z. and J.Z.; formal analysis, Q.G. and H.Z.; investigation, Q.G., H.Z., Z.Y. and S.G.; resources, H.Z.; data curation, Q.G., H.D. and H.Z.; writing—original draft preparation, Q.G. and H.Z.; writing—review and editing, H.Z., S.G., Z.Y. and J.Z.; visualization, Q.G. and H.Z.; supervision, H.Z.; project administration, H.Z.; funding acquisition, H.Z. and X.H. All authors have read and agreed to the published version of the manuscript.

Funding: This work was supported by the Tibet Autonomous Region Science and Technology Plan Project Key Project (XZ202201ZY0003G, XZ202001ZY0056G), The 14th Five-Year Plan National Key Research and Development Program (2021YFD2201302), National Natural Science Foundation of China (31901298), and the Natural Science Foundation of Fujian Province (2021J01059).

Data Availability Statement: Not applicable.

Conflicts of Interest: The authors declare no conflict of interest.

Abbreviations

The following acronyms are used in this manuscript:

UAV	unmanned aerial vehicle
ESP2	estimation of scale parameter 2
RFE	recursive feature elimination
RF	random forest
SVM	support vector machine
KNN	k-nearest neighbor
OA	overall accuracy
Kappa	kappa coefficient
SPEC	spectrum features
INDE	index features
GLCM	texture features
GEOM	geometric features
OOB	out-of-bag
ANN	artificial neural network

References

1. Cheng, X.; Nizamani, M.M.; Jim, C.; Qureshi, S.; Liu, S.; Zhu, Z.; Wu, S.; Balfour, K.; Wang, H. Response of urban tree DBH to fast urbanization: Case of coastal Zhanjiang in south China. *Urban Ecosyst.* **2022**, *25*, 511–522. [CrossRef]
2. Baker, H.J.; Hutchins, M.G.; Miller, J.D. How robust is the evidence for beneficial hydrological effects of urban tree planting? *Hydrol. Sci. J.* **2021**, *66*, 1306–1320. [CrossRef]
3. Pataki, D.E.; Alberti, M.; Cadenasso, M.L.; Felson, A.J.; McDonnell, M.J.; Pincetl, S.; Pouyat, R.V.; Setälä, H.; Whitlow, T.H. The Benefits and Limits of Urban Tree Planting for Environmental and Human Health. *Front. Ecol. Evol.* **2021**, *9*, 603757. [CrossRef]
4. Lumnitz, S.; Devisscher, T.; Mayaud, J.R.; Radic, V.; Coops, N.C.; Griess, V.C. Mapping trees along urban street networks with deep learning and street-level imagery. *ISPRS J. Photogramm.* **2021**, *175*, 144–157. [CrossRef]
5. Sillero, N.; Arenas-Castro, S.; Enriquez Urzelai, U.; Vale, C.G.; Sousa-Guedes, D.; Martínez-Freiría, F.; Real, R.; Barbosa, A.M. Want to model a species niche? A step-by-step guideline on correlative ecological niche modelling. *Ecol. Model.* **2021**, *456*, 109671. [CrossRef]
6. Mo, Y.; Zhong, R.; Cao, S. Orbita hyperspectral satellite image for land cover classification using random forest classifier. *J. Appl. Remote Sens.* **2021**, *15*, 014519. [CrossRef]
7. Ye, Z.; Wei, J.; Lin, Y.; Guo, Q.; Zhang, J.; Zhang, H.; Deng, H.; Yang, K. Extraction of Olive Crown Based on UAV Visible Images and the U2-Net Deep Learning Model. *Remote Sens.* **2022**, *14*, 1523. [CrossRef]
8. Pádua, L.; Vanko, J.; Hruška, J.; Adão, T.; Sousa, J.J.; Peres, E.; Morais, R. UAS, sensors, and data processing in agroforestry: A review towards practical applications. *Int. J. Remote Sens.* **2017**, *38*, 2349–2391. [CrossRef]
9. Ahmadi, P.; Mansor, S.; Farjad, B.; Ghaderpour, E. Unmanned Aerial Vehicle (UAV)-based remote sensing for early-stage detection of Ganoderma. *Remote Sens.* **2022**, *14*, 1239. [CrossRef]
10. Langhammer, J. UAV monitoring of stream restorations. *Hydrology* **2019**, *6*, 29. [CrossRef]
11. Martins, B.H.; Suzuki, M.; Yastika, P.E.; Shimizu, N. Ground surface deformation detection in complex landslide area—bobonaro, Timor-Leste—using SBAS DinSAR, UAV photogrammetry, and field observations. *Geosciences* **2020**, *10*, 245. [CrossRef]
12. Wang, Y.; Wang, J.; Chang, S.; Sun, L.; An, L.; Chen, Y.; Xu, J. Classification of Street Tree Species Using UAV Tilt Photogrammetry. *Remote Sens.* **2021**, *13*, 216. [CrossRef]
13. Bian, L.; Zhang, H.; Ge, Y.; Čepl, J.; Stejskal, J.; EL-Kassaby, Y.A. Closing the gap between phenotyping and genotyping: Review of advanced, image-based phenotyping technologies in forestry. *Ann. Forest Sci.* **2022**, *79*, 22. [CrossRef]
14. Jackson, C.M.; Adam, E. Machine Learning Classification of Endangered Tree Species in a Tropical Submontane Forest Using WorldView-2 Multispectral Satellite Imagery and Imbalanced Dataset. *Remote Sens.* **2021**, *13*, 4970. [CrossRef]
15. Keyport, R.N.; Oommen, T.; Martha, T.R.; Sajinkumar, K.S.; Gierke, J.S. A comparative analysis of pixel- and object-based detection of landslides from very high-resolution images. *Int. J. Appl. Earth Obs.* **2018**, *64*, 1–11. [CrossRef]
16. Myint, S.W.; Gober, P.; Brazel, A.; Grossman-Clarke, S.; Weng, Q. Per-pixel vs. object-based classification of urban land cover extraction using high spatial resolution imagery. *Remote Sens. Environ.* **2011**, *115*, 1145–1161. [CrossRef]
17. Collin, F.D.; Durif, G.; Raynal, L.; Lombaert, E.; Gautier, M.; Vitalis, R.; Marin, J.M.; Estoup, A. Extending approximate Bayesian computation with supervised machine learning to infer demographic history from genetic polymorphisms using DIYABC Random Forest. *Mol. Ecol. Resour.* **2021**, *21*, 2598–2613. [CrossRef]
18. Su, T.; Wu, C.; Kao, J. Artificial intelligence in precision medicine in hepatology. *J. Gastroen. Hepatol.* **2021**, *36*, 569–580. [CrossRef]

19. Georganos, S.; Grippa, T.; Niang Gadiaga, A.; Linard, C.; Lennert, M.; Vanhuysse, S.; Mboga, N.; Wolff, E.; Kalogirou, S. Geographical random forests: A spatial extension of the random forest algorithm to address spatial heterogeneity in remote sensing and population modelling. *Geocarto Int.* **2021**, *36*, 121–136. [CrossRef]
20. Granger, J.E.; Mahdianpari, M.; Puestow, T.; Warren, S.; Mohammadimanesh, F.; Salehi, B.; Brisco, B. Object-based random forest wetland mapping in Conne River, Newfoundland, Canada. *J. Appl. Remote Sens.* **2021**, *15*, 38506. [CrossRef]
21. Wang, X.; Wang, Y.; Zhou, C.; Yin, L.; Feng, X. Urban forest monitoring based on multiple features at the single tree scale by UAV. *Urban For. Urban Green.* **2021**, *58*, 126958. [CrossRef]
22. Fang, G. Application of NCIWI in water body information extraction of city. *Sci. Surv. Mapp.* **2016**, *41*, 44–49.
23. Merzlyak, M.N.; Gitelson, A.A.; Chivkunova, O.B.; Rakitin, V.Y. Non-destructive optical detection of pigment changes during leaf senescence and fruit ripening. *Physiol. Plant.* **1999**, *106*, 135–141. [CrossRef]
24. Baret, F.; Guyot, G. Potentials and limits of vegetation indices for LAI and APAR assessment. *Remote Sens. Environ.* **1991**, *35*, 161–173. [CrossRef]
25. Verstraete, M.M.; Pinty, B.; Myneni, R.B. Potential and limitations of information extraction on the terrestrial biosphere from satellite remote sensing. *Remote Sens. Environ.* **1996**, *58*, 201–214. [CrossRef]
26. LI, X.; Li, H.; Chen, D.; Liu, Y.; Liu, S.; Liu, C.; Hu, G. Multiple Classifiers Combination Method for Tree Species Identification Based on GF-5 and GF-6. *Sci. Silvae Sin.* **2020**, *56*, 93–104.
27. Gamon, J.A.; Surfus, J.S. Assessing leaf pigment content and activity with a reflectometer. *New Phytol.* **1999**, *143*, 105–117. [CrossRef]
28. Person, R.S.; Kudina, L.P. Discharge frequency and discharge pattern of human motor units during voluntary contraction of muscle. *Electroencephalogr. Clin. Neurophysiol.* **1972**, *32*, 471–483. [CrossRef]
29. Huete, A.; Didan, K.; Miura, T.; Rodriguez, E.P.; Gao, X.; Ferreira, L.G. Overview of the radiometric and biophysical performance of the MODIS vegetation indices. *Remote Sens. Environ.* **2002**, *83*, 195–213. [CrossRef]
30. Ma, W. Winter Wheat Nitrogen Nutrition Diagnosis Based on the UAV Remote Sensing. Master's Thesis, Henan Polytechnic University, Jiaozuo, China, 2017.
31. Zhao, C.; Huang, M.; Huang, W.; Liu, L.; Wang, J. Analysis of Winter Wheat Stripe Rust Characteristic Spectrum and Establishing of Inversion Models. In Proceedings of the 2004 IEEE International Geoscience and Remote Sensing Symposium, Anchorage, AK, USA, 20–24 September 2004; Volume 6, pp. 4318–4320.
32. Gitelson, A.A.; Kaufman, Y.J.; Stark, R.; Rundquist, D. Novel algorithms for remote estimation of vegetation fraction. *Remote Sens. Environ.* **2002**, *80*, 76–87. [CrossRef]
33. Rondeaux, G.; Steven, M.; Baret, F. Optimization of soil-adjusted vegetation indices. *Remote Sens. Environ.* **1996**, *55*, 95–107. [CrossRef]
34. Zhou, R.; Yang, C.; Li, E.; Cai, X.; Yang, J.; Xia, Y. Object-Based Wetland Vegetation Classification Using Multi-Feature Selection of Unoccupied Aerial Vehicle RGB Imagery. *Remote Sens.* **2021**, *13*, 4910. [CrossRef]
35. Islam, N.; Rashid, M.M.; Wibowo, S.; Xu, C.; Morshed, A.; Wasimi, S.A.; Moore, S.; Rahman, S.M. Early Weed Detection Using Image Processing and Machine Learning Techniques in an Australian Chilli Farm. *Agriculture* **2021**, *11*, 387. [CrossRef]
36. Luo, C.; Qi, B.; Liu, H.; Guo, D.; Lu, L.; Fu, Q.; Shao, Y. Using Time Series Sentinel-1 Images for Object-Oriented Crop Classification in Google Earth Engine. *Remote Sens.* **2021**, *13*, 561. [CrossRef]
37. Mäyrä, J.; Keski-Saari, S.; Kivinen, S.; Tanhuanpää, T.; Hurskainen, P.; Kullberg, P.; Poikolainen, L.; Viinikka, A.; Tuominen, S.; Kumpula, T.; et al. Tree species classification from airborne hyperspectral and LiDAR data using 3D convolutional neural networks. *Remote Sens. Environ.* **2021**, *256*, 112322. [CrossRef]
38. Ye, Z.; Guo, Q.; Zhang, J.; Zhang, H.; Deng, H. Extraction of urban impervious surface based on the visible images of UAV and OBIA-RF algorithm. *Trans. Chin. Soc. Agric. Eng.* **2022**, *38*, 225–234.
39. Garg, R.; Kumar, A.; Prateek, M.; Pandey, K.; Kumar, S. Land cover classification of spaceborne multifrequency SAR and optical multispectral data using machine learning. *Adv. Space Res.* **2022**, *69*, 1726–1742. [CrossRef]
40. Talukdar, S.; Singha, P.; Mahato, S.; Pal, S.; Liou, Y.A.; Rahman, A. Land-use land-cover classification by machine learning classifiers for satellite observations—A review. *Remote Sens.* **2020**, *12*, 1135. [CrossRef]
41. Fu, B.; Liu, M.; He, H.; Lan, F.; He, X.; Liu, L.; Huang, L.; Fan, D.; Zhao, M.; Jia, Z. Comparison of optimized object-based RF-DT algorithm and SegNet algorithm for classifying Karst wetland vegetation communities using ultra-high spatial resolution UAV data. *Int. J. Appl. Earth Obs.* **2021**, *104*, 102553. [CrossRef]
42. Zhao, F.; Wu, X.; Wang, S. Object-oriented Vegetation Classification Method based on UAV and Satellite Image Fusion. *Procedia Comput. Sci.* **2020**, *174*, 609–615. [CrossRef]
43. Sothe, C.; Dalponte, M.; Almeida, C.M.D.; Schimalski, M.B.; Lima, C.L.; Liesenberg, V.; Miyoshi, G.T.; Tommaselli, A.M.G. Tree species classification in a highly diverse subtropical forest integrating UAV-based photogrammetric point cloud and hyperspectral data. *Remote Sens.* **2019**, *11*, 1338. [CrossRef]
44. Dobrinić, D.; Gašparović, M.; Medak, D. Sentinel-1 and 2 Time-Series for Vegetation Mapping Using Random Forest Classification: A Case Study of Northern Croatia. *Remote Sens.* **2021**, *13*, 2321. [CrossRef]
45. Abdollahnejad, A.; Panagiotidis, D. Tree species classification and health status assessment for a mixed broadleaf-conifer forest with UAS multispectral imaging. *Remote Sens.* **2020**, *12*, 3722. [CrossRef]